ELSEVIER

Journal of Alloys and Compounds 434–435 (2007) 248–251

Journal of ALLOYS AND COMPOUNDS

www.elsevier.com/locate/jallcom

Pecularities of electrical resistivity during transformations in amorphous and nanocrystalline alloys

M. Deanko [a], M. Paluga [a], D.M. Kepaptsoglou [b], D. Muller [a], P. Mrafko [a], D. Janičkovič [a], E. Hristoforou [b], I. Škorvánek [c], P. Švec [a,*]

[a] *Institute of Physics, Slovak Academy of Sciences, Dúbravská cesta 9, 845 11 Bratislava, Slovakia*

[b] *Laboratory of Physical Metallurgy, National Technical University of Athens, 9 Heroon Polytechniou Street, Zografou Campus, 15780 Athens, Greece*

[c] *Institute of Experimental Physics, Slovak Academy of Sciences, Watsonova 47, 043 53 Košice, Slovakia*

Available online 17 October 2006

Abstract

Classical transformations from rapidly quenched amorphous into (nano)crystalline state monitored by time and temperature evolution of electrical resistivity are discussed as a typical case. Common and different features observed in these transformations, related to local structural and chemical arrangements, are compared with special cases, e.g. sharp increase of resistivity during energy-intensive crystallization observed in Fe–Ni based amorphous systems. A drastic increase of electrical resistivity during transformation in Al–V system is attributed to the formation of nanoquasicrystalline structures with a predicted pseudogap in the electron density at the Fermi level. The results are correlated with microstructure observations and with data from routinely used methods of kinetic analysis with respect to the expected local atomic ordering in amorphous precursor systems.

PACS: 64.70.Nd; 72.15.Cz; 61.43.Dq

Keywords: Metallic glasses; Fe–Ni–Nb–B alloys; Al–V alloys; Electrical resistivity; Nanocrystallization

1. Introduction

Electrical resistivity of metallic systems represents a property sensitive to their electronic structure, availability of charge carriers in the system and mechanisms of their scattering. The physics behind these effects, in turn, reflects important information about the spatial ordering of atoms and their interactions. Moreover, the effect of enhanced bonding, ranging from purely metallic to more directional and stronger bonds in specific cases of amorphous systems, can manifest itself in anomalous behaviour of the electrical resistivity. This is especially visible in transformations from amorphous state and in the course of formation of nanometer-sized phases with specific structure and composition.

In most cases the values of specific electrical resistivity ρ in amorphous systems lie in the range of 50–250 $\mu\Omega$ cm, with the corresponding temperature coefficient α given as $\rho(T)/\rho(T_0) = R(T)/R(T_0) = 1 + \alpha(T - T_0)$, where $R(T_0)$ and $\rho(T_0)$, are the values of electrical resistance or specific electrical resistivity, respectively, at T_0, usually 300 K. The values of α are of the order of 10^{-4} K^{-1} and decrease with increasing ρ, attaining negative values for $\rho > \sim 150$ $\mu\Omega$ cm. The corresponding values of ρ in crystalline counterparts are generally lower, with higher α. In such cases subsequent transformations by nucleation and growth mechanisms from amorphous into partial or fully crystalline states lead to a decrease of electrical resistivity, its value being given by the serial model [1] and [2] (where the necessary and sufficient conditions for its use were discussed in detail) as a weighted sum of the contributions of ρ of the respective amorphous and crystalline phases, the volume content of each phase being the weighting factor. In most cases the change (decrease) does not exceed few tens of percents of the initial value.

The necessary condition for the use of the serial model is the validity of the same rule for the evolution of α with proceeding transformation. Serial model has been successfully tested using finite-element computations on structures with different crystallinity content, x, obtained by simulation of nucleation and growth [3] of phases having ρ of similar magnitudes. The model can be checked experimentally [4] on real systems by

* Corresponding author. Tel.: +421 2 5941 0561; fax: +421 2 5477 6085.
E-mail address: fyzisvec@savba.sk (P. Švec).

0925-8388/$ – see front matter © 2006 Elsevier B.V. All rights reserved.
doi:10.1016/j.jallcom.2006.08.124

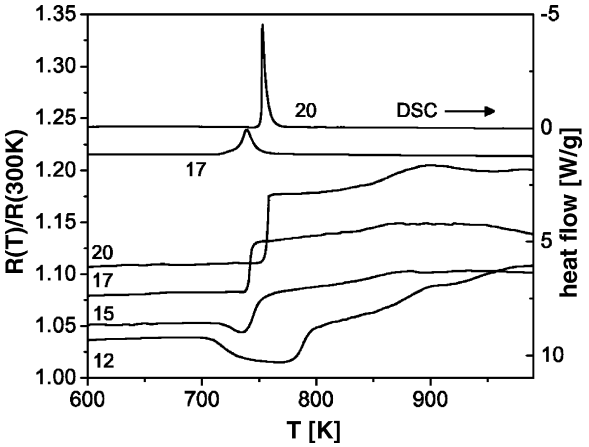

Fig. 1. Temperature dependence of normalized electrical resistivity $R(T)/R(300\,K)$ and DSC traces of $(Fe_1Ni_3)_{81-x}Nb_7B_x$ for $x = 12, 15, 17, 20$ (numbers in the graph indicate B content) taken at 10 K/min.

independent estimations of x using quantitative structure analysis [2,3] or comparative measurements by classical methods of thermal analysis. The advantage of using time and temperature dependencies $R(T, t)$ for kinetic and thermodynamic analyses is high attainable precision of its determination; resistivity is a physical property present from the initial to final stages of the transformations, which can then be monitored over a huge range of isothermal annealing times [5] or heating rates without loss of measurement accuracy. Furthermore, high precision allows detection of minute changes of R, providing thus a very sensitive tool for detecting special effects related to small contents of different phases or small changes of R, especially under additional external influences, e.g. magnetic field or applied strain [6]. Special attention below will be given to transformations where the forming phases exhibit higher ρ than the initial rapidly quenched amorphous structure.

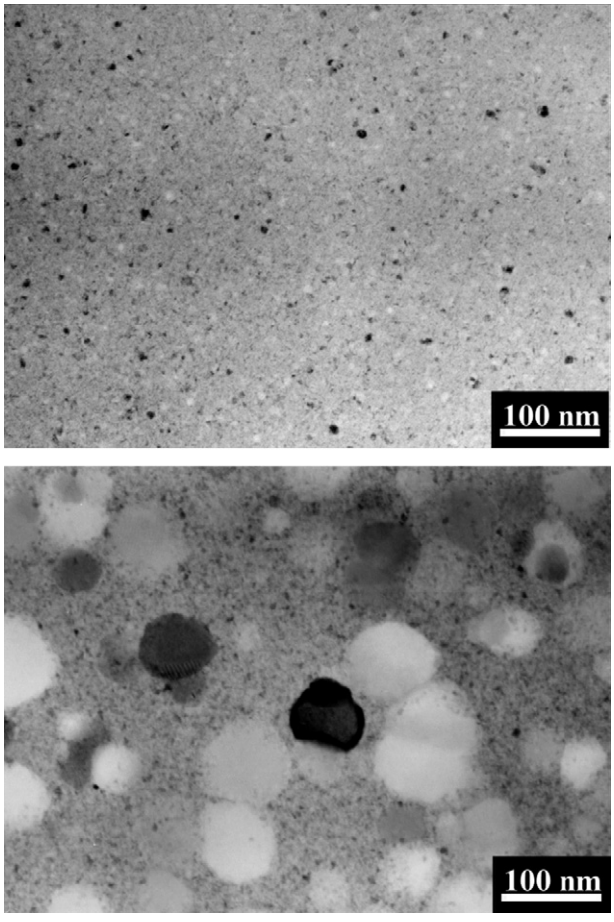

Fig. 2. Formation of nanosized bcc-FeNi grains embedded in amorphous matrix in $(Fe_1Ni_3)_{81}Nb_7B_{12}$ after annealing at 823 K for 1 h (top) and simultaneous formation of bcc-FeNi nanograins together with substantially larger $(FeNi)_{23}B_6$ in $(Fe_1Ni_3)_{76}Nb_7B_{17}$ after annealing at 773 K for 1 h (bottom).

2. Transformations in amorphous Fe–Ni–Nb–B systems

Amorphous ribbons $(Fe_1Ni_3)_{81-x}Nb_7B_x$ for $x = 12, 15, 17, 20$ were prepared by planar flow casting. Their transformation into nanocrystalline state is well reflected by a change of $R(T)$ (Fig. 1). For lower B content the formation of nanocrystalline bcc-FeNi (Fig. 2) is accompanied by a small decrease of $R(T)$. Second transformation stage above 800 K leads to crystallization of remaining amorphous matrix into a mixture of small amount of borides and fcc-$(FeNi)_{23}B_6$. Higher B content changes significantly the transformation kinetics, which becomes much narrower in temperature and time. This is manifest by a small but sharp increase of $R(T)$. The transformation leads to a single-step formation of a mixture of bcc-FeNi nanograins together with larger fcc-$(FeNi)_{23}B_6$ grains (Fig. 3). The morphology, however,

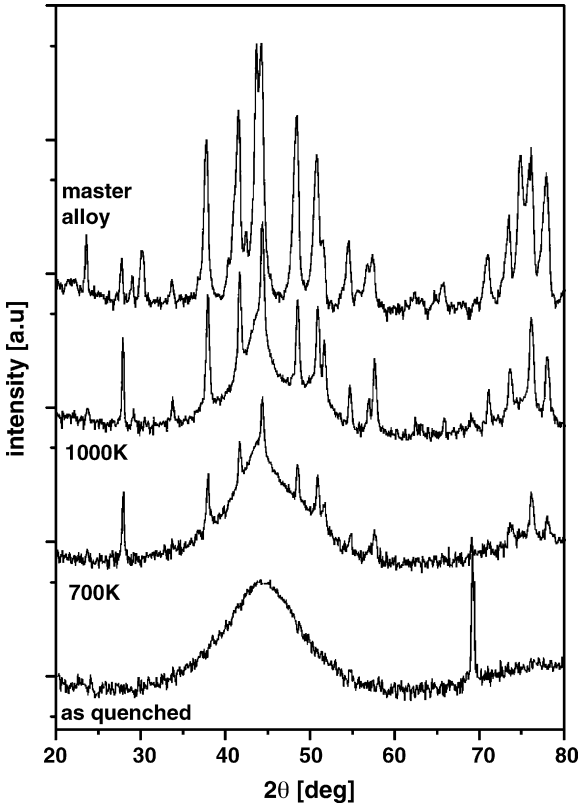

Fig. 3. X-ray diffraction patterns of as-quenched and annealed $(Fe_1Ni_3)_{76}Nb_7B_{17}$. Simultaneous formation of bcc-FeNi and fcc-$(FeNi)_{23}B_6$ with slightly smaller lattice parameter than that of pure $Fe_{23}B_6$ is observed.

still resembles the nucleation-and-growth type of crystallization and no significant impingement of the grains is observed even in the later stages. Sharp DSC peak attaining ~4 W/g is observed during the transformation. No further reaction (except grain coarsening visible in TEM) seems to be taking place up to ~1000 K as monitored by both $R(T)$ and DSC. It is to be noted that the phases formed in the single-step transformation are identical to those observed in the precursor master alloy, allowing to assume that the local ordering of both the precursor alloy and the rapidly quenched amorphous ribbons with higher B content are rather similar, facilitating nucleation and growth processes directly into more stable crystalline phases.

3. Transformations in Al–V

The Al–V alloy ribbons with composition $Al_{90}V_{10}$ have been prepared by planar flow casting and subsequently have been subjected to linear heating measurements of ρ under different heating regimes from room temperatures to ~1100 K (Fig. 4), well above the melting temperature of pure Al, $T_{M,Al}$. Transmission electron microscopy (TEM) and X-ray diffraction (Fig. 5) of as-quenched samples show, besides amorphous halo, the presence of nanocrystalline Al grains and ~100 nm sized crystals

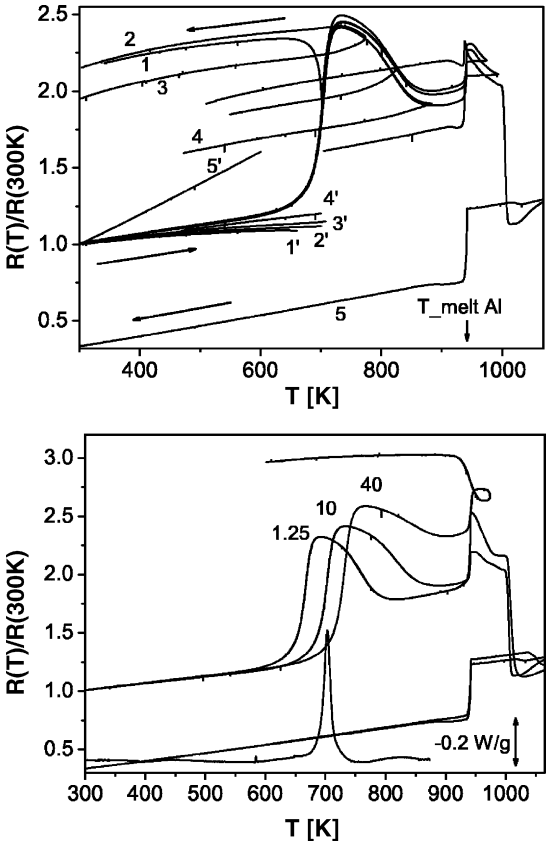

Fig. 4. Top: temperature dependence of normalized electrical resistivity $R(T)/R(300\,K)$ of as-quenched $Al_{90}V_{10}$ samples during 10 K/min linear heating to different temperatures. Selected cooling runs 1 to 5 renormalized to 300 K are redrawn as 1′ to 5′. Bottom: shift of $R(T)/R(300\,K)$ during formation of $Al_{10}V$ phase at heating rates of 1.25, 10 and 40 K/min; DSC trace at 10 K/min is shown for comparison.

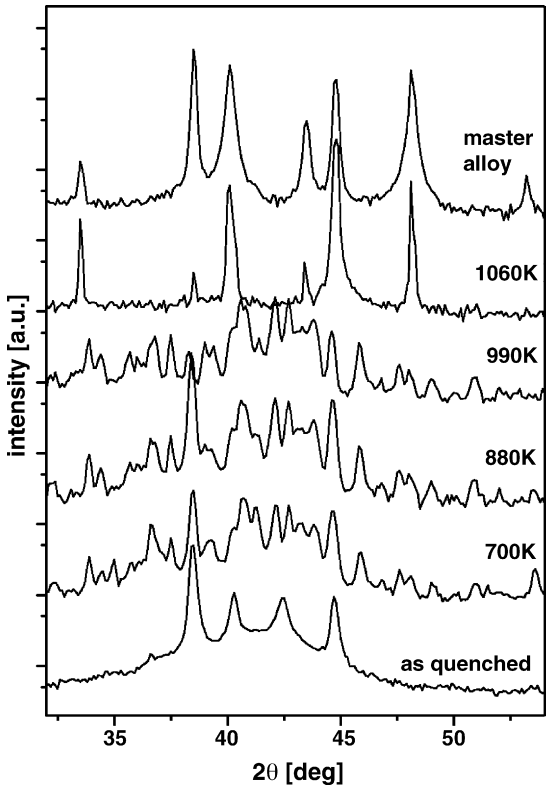

Fig. 5. XRD patterns of $Al_{90}V_{10}$ samples in as-quenched and annealed states as per Fig. 4 showing evolution of as-quenched structure containing amorphous phase and fcc-Al nanograins in crystalline $Al_{86}V_{14}$ into $Al_{10}V$ and small amounts of $Al_{47}V_7$ above 700 K. The phases remain stable up to 1000 K, above which the formation of Al and Al_3V is observed, the same as in the master alloy.

identified as $Al_{86}V_{14}$. Heating above 700 K leads to formation of $Al_{10}V$ phase with large lattice parameter, which has been investigated in detail in [7]. Different types of interatomic Al–V bonds in this phase with enhanced charge density and degree of localization (pseudogap at Fermi level) were shown to lead, besides affecting other properties, to values of ρ as high as ~1000 μΩ cm. The values of ρ of the as-quenched ribbon were determined to be 85 ± 15 μΩ cm, the error being mainly due to geometrical irregularities of the ribbon surface. The increase of $R(T)/R(300\,K)$ to almost 250% at the temperatures between 650 and 750 K reflects the process of formation of the highly resistive $Al_{10}V$ phase at the expense of both Al and $Al_{86}V_{14}$, as shown in Fig. 5. A Kissinger-type activation energy of 206 ± 16 kJ/mol has been estimated for this transformation from the shift of peaks of temperature derivatives of $R(T)$ to higher values (Fig. 4, bottom) with increasing heating rate; this is a typical effect analogous to the one observed in DSC scans. No heating rate dependence is observed on $R(T)$ below ~600 K.

Heating to temperatures up to 1000 K, even above $T_{M,Al}$, does not significantly affect the presence of the $Al_{10}V$ phase; only small amounts of additional phase identified by XRD as $Al_{43}V_7$ are formed. Final transformation into Al and Al_3V accompanied by irreversible drop of electrical resistivity takes place above 1000 K. Incidentally, these two phases are the only ones found present in the precursor master alloy used for ribbon preparation. Large increase of $R(T)$ together with insensivity of temperature

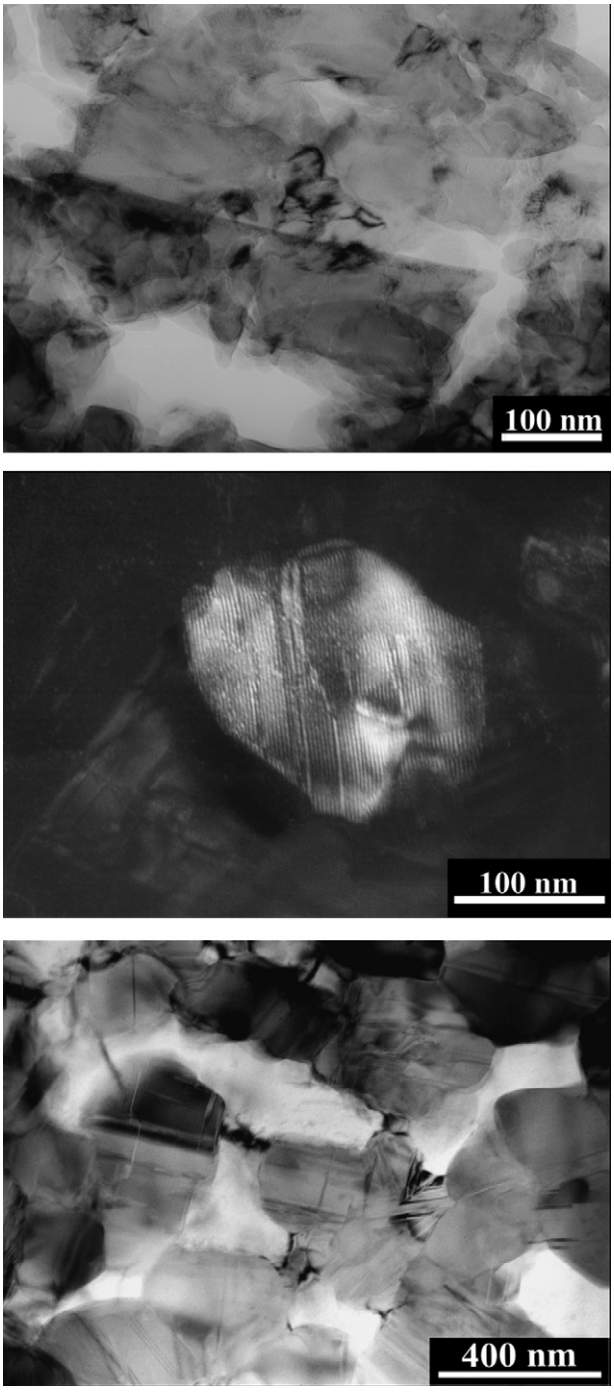

Fig. 6. The evolution of morphology of $Al_{90}V_{10}$ from as-quenched state (top) containing amorphous phase and nano-Al embedded in $Al_{86}V_{14}$ into $Al_{90}V_{10}$ (middle) and further into a skeleton of interconnected $Al_{90}V_{10}$ grains with electrically more conducive channels (bottom).

dependencies of $R(T)$ after the formation of $Al_{10}V$ (plotted in Fig. 4 as curves 1′ to 4′ renormalized to 300 K) indicates that the resistivity of the transformed system differs from the behaviour predicted by the serial model. The matrix in this case is composed of a significant amount of highly resistive phase with the remains of Al and forming $Al_{43}V_7$ embedded in the matrix. Thus the effective conductivity (or rather its decrease) seems to be due to the conductive paths formed by these phases in the channels between the interconnected grains of $Al_{10}V$; the effect of formation of $Al_{10}V$ effectively decreases the originally conductive cross-section of the ribbon sample. Such a picture is in accord with the evolution of morphology shown in Fig. 6 where large grains of $Al_{10}V$ become mutually interconnected as the transformation proceeds, forming a (highly resistive) skeleton with interconnecting (conductive) channels of the remaining metallic Al and $Al_{43}V_7$.

In order to test the presence and effect of the predicted pseudogap in $Al_{10}V$ the *I–V* (current–voltage) characteristics of samples heated up to the temperatures indicated in Fig. 4 were measured in quasistatic mode at 300 and 800 K for a broad range of exciting currents (10^{-10} to 10^{-2} A). to assess the eventual semiconducting contribution to electron transport. However, neither the *I–V* (linear) nor the *R–V* (constant) dependencies suggested any anomaly in the conduction mechanism.

4. Conclusions

Time and temperature dependencies of electrical resistivity represent a valuable and sensitive tool for investigating effects related to atomic and electron structure in amorphous metallic systems and during their transformations into (nano)crystalline states. High sensitivity and attainable accuracy of such measurements together with possibilities to perform measurements under extreme external parameters as e.g. high heating rates, short isothermal onset times, prolonged isothermal measurements, etc., predestine resistometry for analysis of fine effects and for kinetic analysis over a broad range of temperatures. Direct quantification of phase transformations, however, has to be performed in each case to verify and calibrate the relationship between the evolution of new phases and the model used to recompute the corresponding changes of electrical resistivity. Special care should be taken especially in the cases where large difference between the resistivities of initial and final phases are expected and where the morphology and mechanisms differ from those of classical nucleation-and-growth from (amorphous) matrix with low degree of impingement.

Acknowledgments

Acknowledgements are due to the Slovak GAS (VEGA 5/5096/25, APVT-51-052702, APVT-99-017904), CEX “Nanosmart” and to the PENED 2001-01ED93 of the Hellenic GSRT.

References

[1] R. Landauer, J. Appl. Phys. 23 (1952) 779.
[2] P. Svec, K. Kristiakova, Mater. Sci. Forum 360–362 (2001) 475–480.
[3] M. Deanko, Ph.D. Thesis, Bratislava, 2006.
[4] H.K. Lachowicz, M. Kuzminski, T. Kulik, A. Hernando, Nanostruct. Mater. 4 (1994) 865.
[5] D.M. Kepaptsoglou, et al., this volume.
[6] D.M. Kepaptsoglou, K. Efthimiadis, P. Svec, E. Hristoforou, J. Magn. Magn. Mater. 304 (2006) e583–e585.
[7] M. Jahnatek, M. Krajci, J. Hafner, Phys. Rev. B 71 (2005) 024101.